Space Observation of Carbon Dioxide Partial Pressure at Ocean Surface

W. Timothy Liu, *Senior Member, IEEE*, and Xiaosu Xie

***Abstract*—We have developed and validated a statistical model to estimate the partial pressure (or fugacity) of carbon dioxide at the sea surface from space-based observations of sea surface temperature, chlorophyll, and salinity. More than a quarter million *in situ* measurements coincident with satellite data were compiled. A portion of the data was randomly selected to train and validate the model. We have produced and made accessible nine years (2002–2011) of the partial pressure at 0.5° and daily resolutions over the global oceans. The outputs are found to be sensitive to variability from intraseasonal to interannual time scales and from the equatorial to high-latitude oceans. They can capture known phenomena, such as, annual spring blooms at high latitudes, interannual episodes of El Niño, and westward propagation of tropical instability waves. The feasibility of using a single algorithm to map the partial pressure over global oceans for all seasons is demonstrated. The result is important for characterizing the sources and sinks of atmospheric greenhouse gas and ocean biogeochemistry. We discuss the significance of the Advanced Scanning Microwave Radiometer in the consistent measurement of sea surface temperature, which is the main driver of ocean carbon dioxide change, in cold and warm waters, under clear and cloudy sky. The continuous and consistent coverage of the partial pressure over global ocean using space-based data is discussed.**

***Index Terms*—Acidification, carbon dioxide (CO2), chlorophyll, greenhouse warming, salinity, satellite measurements, sea surface temperature (SST).**

I. Introduction

CARBON and water cycles are important to weather, climate, ecology, and human livelihood. The two cycles are closely linked. The alarmingly rapid increase of global atmospheric carbon dioxide (CO_2) content has been well documented [1] and is ascribed as the main factor in global warming. The net influx of CO_2 to the ocean causes change in the carbonate system, referred to as ocean acidification. Significant acidification will be deleterious to many marine life forms and ecosystems. We know approximately that oceans absorbed 26% of the CO_2 we emitted between 2005 and 2014 [2], and ocean's acidity increases by 26% since the start of the industrial revolution [3], but we know much less about the temporal-spatial distribution of the CO_2 exchange. The CO_2 partial pressure at ocean surface is critical in determining the exchange.

The net CO_2 flux between the ocean and the atmosphere has been parameterized in terms of a transfer (piston) velocity and (ΔpCO_2), which is the difference between the partial pressure of CO_2 in the sea (pCO_2s) and that in the air (pCO_2a) near the surface. The modeling of the transfer velocity in term of wind speed has been extensively investigated, and the advantage of space-based measurement of wind speed in providing the needed temporal and spatial resolutions have been demonstrated [4]–[8]. With the new perspective of retrieving ocean surface stress and roughness directly from measured backscatter [9], by-passing wind retrieval, improvement of piston velocity estimation is being pursued [10], [11]. Other factors, such as surfactant [12]–[15], and bubbles [16] have also been studied. Oceanic processes have smaller spatial scales than atmospheric processes, and the result is that pCO_2a has less spatial variability than pCO_2s. The annual ranges (annual maximum–minimum) of pCO_2a are much less than those of pCO_2s over most of the oceans [17]. It is generally believed that pCO_2a has much less temporal changes than pCO_2s. This study is focused on the estimation of pCO_2s.

In many studies, the fugacity of CO_2 (fCO_2) is used in place of pCO_2 to distinguish between the real partial pressure instead of the partial pressure of an ideal gas. For an ideal gas, fugacity equals partial pressure. The conversion of one to another requires knowledge of pressure, temperature, and mole fraction of CO_2 in dry air (xCO_2) [18]. The difference between fCO_2 and pCO_2 is generally small compared with the uncertainties of our model output. For fixed pressure at 1013 mb and xCO_2 of 350 ppm, changing temperature from –5 °C to 30 °C changes the differences between fCO_2 and pCO_2 by less than 0.2%. With fixed temperature at 25 °C and $xCO_2 = 350$ ppm, changing p from 1013 to 900 mb changes the differences between fCO_2 and pCO_2 by less than 0.3%. This study is directed to pCO_2.

pCO_2s has been measured largely on ships (see Section IV). The conventional methods are not sufficient to characterize spatial and temporal variability. There were efforts to relate pCO_2s to more readily available measurements, which are believed to be drivers of pCO_2s variation. The variation of the ocean surface carbon system parameters and the relations among them are mainly driven by thermodynamics. Water temperature controls the solubility of CO_2 and is a main driver. Biological activity is another obvious driver. Removal and addition of CO_2 by plankton photosynthesis or respiration is a significant cause of

Manuscript received December 15, 2016; revised March 7, 2017, July 18, 2017, and August 21, 2017; accepted October 14, 2017. Date of publication December 14, 2017; date of current version December 19, 2017. This work was supported by the JPL Research and Technology Development Program and the NASA Ocean Surface Salinity Science Team. *(Corresponding author: W. Timothy Liu.)*

The authors are with the Jet Propulsion Laboratory, California Institute of Technology, Pasadena, CA 91109 USA (e-mail: w.t.liu@jpl.nasa.gov; xiaosu.xie@jpl.nasa.gov).

Digital Object Identifier 10.1109/JSTARS.2017.2766138

the variation. Chlorophyll is essential in photosynthesis, allowing plants to absorb energy from light. The measurement of chlorophyll-*a* (Chl-*a*) is used as an indication of biological activity. Sea surface salinity (SSS) is known to be closely related to alkalinity and is also an important driver, particularly over regions with strong fresh water input near river discharge and where significant difference between evaporation and precipitation exits. Previous empirical formula to relate pCO_2s to these parameters and their deficiencies are discussed in Section II.

We have been collecting *in situ* measurements of pCO_2s for decades, starting with those from the cruises of the Joint Global Ocean Flux Study and World Ocean Circulation Experiment, in parallel with other national and international efforts. In 2011, we decided to collocate them with space-based measurements of sea surface temperature (SST) and Chl-*a* to train a model for deriving pCO_2s [20]. Space-based SSS measurements were not sufficient and climatology was used. Satellites offer continuous synoptic views of the ocean and we assume their observations reflect the temporal-spatial variations of pCO_2s.

The quantification of the long-term rise in atmospheric greenhouse gas and global warming is a very important justification to determine pCO_2s. The difficulty of building continuous and consistent long time series of satellite observations makes it difficult to address the climate problem. Satellite observations, however, are most useful in characterizing temporal-spatial variations over the global oceans from intraseasonal to interannual time scales. Beside the change of atmospheric CO_2 accumulation, pCO_2s is also needed to study the changes in ocean biogeochemistry, which is not confined to climate scale. The ocean carbon system is described by four key parameters: pCO_2s, pH (a scale to specify acidity or basicity of sea water), total alkalinity, and dissolved inorganic carbon. Knowing two of them will be sufficient to solve the chemical equations for the whole system [19].

The tool to build the statistical model is described in Section III. The collected *in situ* measurements and the collocated space-based data to train the model are summarized in Sections IV and V. The statistical model and its validation with the ensemble data are described in Section VI. The best validation is through applications. The capability of the data in describing the seasonal cycles from the subtropical to extratropical oceans, the spring bloom in the high-latitude oceans, the interannual anomalies associated with El Niño, and the propagation of the intraseasonal tropical instability waves (TIW) in the equatorial Pacific are demonstrated in Section VII.

II. Traditional Methods and Deficiency

Space-based sensors do not measure the flux or pCO_2s directly. Attempts have been made to establish regional and seasonal relations between pCO_2s and variables that are more readily measured. For example, Stephens *et al*. [21] produced a statistical relation between pCO_2s and SST from nine cruises across the Pacific between 1984 and 1989. He concluded that the relation is sufficient to estimate pCO_2s from satellite SST over the oligotrophic subtropical Pacific, but not over the eutrophic Northwest Pacific, with significant primary production. Many algorithms to relate pCO_2s to SST followed, in the Arabian Sea [22], in the Greenland Sea [23], in the Sargasso Sea [24], and in the equatorial Pacific [25], but their applicability is limited by geographical region, season, and time scale, depending on the data used to develop the relation. Chl-*a* was added to SST in later studies, in North Pacific [26] and South China Sea [27]. Sarma *et al*. [28] used meridional transects to build algorithms via dissolved inorganic carbon, using multivariate linear regression, but they computed basin-wide, monthly maps using satellite data and found large discrepancies in some regions of the ocean basin. Instead of developing the algorithm using only *in situ* measurement, Padin *et al*. [29] were the first one to regress *in situ* measurement of pCO_2s with overpass satellite observations of SST and Chl-*a*, but this was only limited to cruises in the Bay of Biscay. Salinity and alkalinity are also related to pCO_2s in some of these studies. These studies mostly use multiple linear regression or polynomials.

The neural network approach was later applied to estimate pCO_2s. Lefevre *et al*. [30] compared two methods: neural network and linear regression in deriving the monthly distribution of pCO_2s in the Atlantic subpolar gyre. The neural network approach has better accuracy with root-mean-square (RMS) error of 3–11 μatm. Telszewski *et al*. [31] derived the monthly pCO_2s in the North Atlantic by applying a self-organizing map neural network; the RMS error was 11.6 μatm. Friedrich and Oschlies [32] estimated and validated monthly pCO_2s in the North Atlantic, using a self-organizing neural network trained by outputs from a biogeochemical model. The monthly pCO_2s had an RMS error of 15.9 μatm.

In almost all studies, the relationships between pCO_2s and other parameters are developed with coincident measurements on cruises, mostly covering a limited region and a particular season. The correlation coefficients between pCO_2s and oceanic parameters change from positive to negative over various regions, as revealed by the correlation maps in Section VII-A. A single universal linear or polynomial regression, as derived in these studies, would not work over the global oceans across all seasons. Multiple relations covering different regions and seasons would have strong boundary discontinuity problems. Based on support vector regression (SVR) as described in Section III, with location and time (season) as input parameters, we have developed a universal model for continuous and global coverage, as described in Section VI.

III. Support Vector Regression

Support vector machine (SVM) is used in this study to derive pCO_2s using space-based observations. Major applications of SVMs include classification, regression, and time series prediction. The SVMs for regression are referred as SVR, which derives the relationship between input and output. A comprehensive tutorial of SVR was given by Smola and Schölkopf [33].

The mathematical expressions of SVM are summarized by Xie *et al*. [34]. The theoretical basis of SVMs originates from statistical learning theory [35]. SVMs essentially translate a nonlinear problem to a linear one by mapping the input into

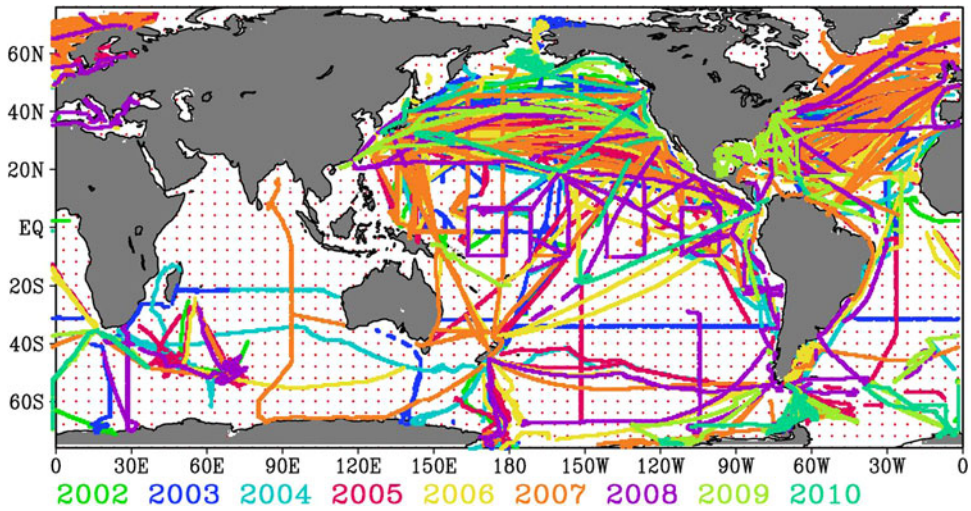

Fig. 1. Collocated pCO_2s measurements with satellite observations during 2002–2010. The pCO_2s data came from all sources available in 2012, as described in Section IV.

a high-dimensional feature space, and fit a linear model in the feature space. The solution of the optimization is unique, which overcomes the problem of converging to locally optimal solutions suffered by neural networks, although neural network can be competitive if it is optimally set up for some applications. The approach is relatively easy to use, because there are only a few parameters to adjust. The simple setting of SVR, with the data training only based on support vectors, avoids over-fitting of the training data. By using the standard quadratic programming algorithms, only one global optimum is achieved. Mapping inputs into high-dimensional feature space and introducing a kernel function can solve the nonlinear relationship between inputs and outputs by turning a nonlinear regression into a linear fitting.

For the regression algorithms in this study, a large training dataset is needed in order to represent global coverage with space and time dependencies. The accuracy of SVR depends on selection of the two hyper-parameters and the kernel parameter to optimize the retrieval algorithms [34]. The initial values of the parameters are empirically estimated from the training data based on previous studies. Then only one parameter varies until the optimized correlation between the trained output and the measurement data is found. Xie *et al*. [34] have demonstrated that SVMs outperform linear regression and neural network in estimating moisture advection by reducing the bias and the standard deviation in comparison with observations, and the results include more accurate extreme values.

IV. *In Situ* Measurements

The *in situ* measurements of surface ocean pCO_2s used to train and validate the statistical model are collected from various available sources. The database archived at the Lamont–Doherty Earth Observatory (LDEO) contains a large part of the pCO_2s measurements, which have been contributed by many institutions from the United States and other countries. Approximately 6.7 million surface ocean pCO_2s observations were made from 1957 to 2012 [36]. The *in situ* dataset also include those from these programs: the global Volunteer Observing Ship project, the Global CO_2 Time-series and Moorings Project, the International Climate Variability Program Global Ocean Carbon and Repeat Hydrography Program, the Global Coastal Carbon DATA Project along the east/west coasts of North America and European coasts, the GLobal Ocean Data Analysis Project, cruises over the Pacific from PACIFic ocean Interior CArbon, ongoing cruise measurements conducted by the Atlantic Oceanographic and Meteorological Laboratory and the Pacific Marine Environmental Laboratory (PMEL), the open ocean moorings and coastal observation network developed by PMEL, the CARbon dioxide IN the Atlantic Ocean (CARINA) data synthesis project [37], and the North Pacific Marine Science Organization. The LDEO database partly overlaps with these data. All data are distributed through the Carbon Dioxide Information Analysis Center (CDIAC). The CARINA data output of total dissolved inorganic carbon (TCO_2) [38] was converted to pCO_2s following the program developed for CO_2 systems by Lewis and Wallace [39], along with alkalinity, temperature, salinity, and pressure. The calculated pCO_2s data are only a very small portion of the measured data.

Our dataset was presented at the inaugural meeting of the Surface Ocean CO_2 Atlas (SOCAT) at UNESCO, Paris, in 2011 [40]. SOCAT is an international program to collect and manage all publicly available underway pCO_2s data from the global oceans [41]. Much of our data overlaps with and is a major part of SOCAT collection. We absorbed additional data from SOCAT and made use of their data control protocol after the meeting. We were able to compile about 250 000 quality-controlled measurements between 2002 and 2010, coincident with satellite measurements of SST and Chl-*a*, as shown in Fig. 1.

Time series at four stations are used to evaluate the data products. The station locations are marked in Fig. 2(a). Monthly measurements for 9 years are from the Hawaii Ocean Time-series (HOT) [42] at Station ALOHA (22°45'N, 158°00'W) and the Bermuda Atlantic Time-series Study (BATS) [43] near Bermuda (64 °W, 32 °N). Data at the Kuroshio Extension Observatory (KEO) at 32.4 °N, 11.6 °E and the Japanese Kuroshio

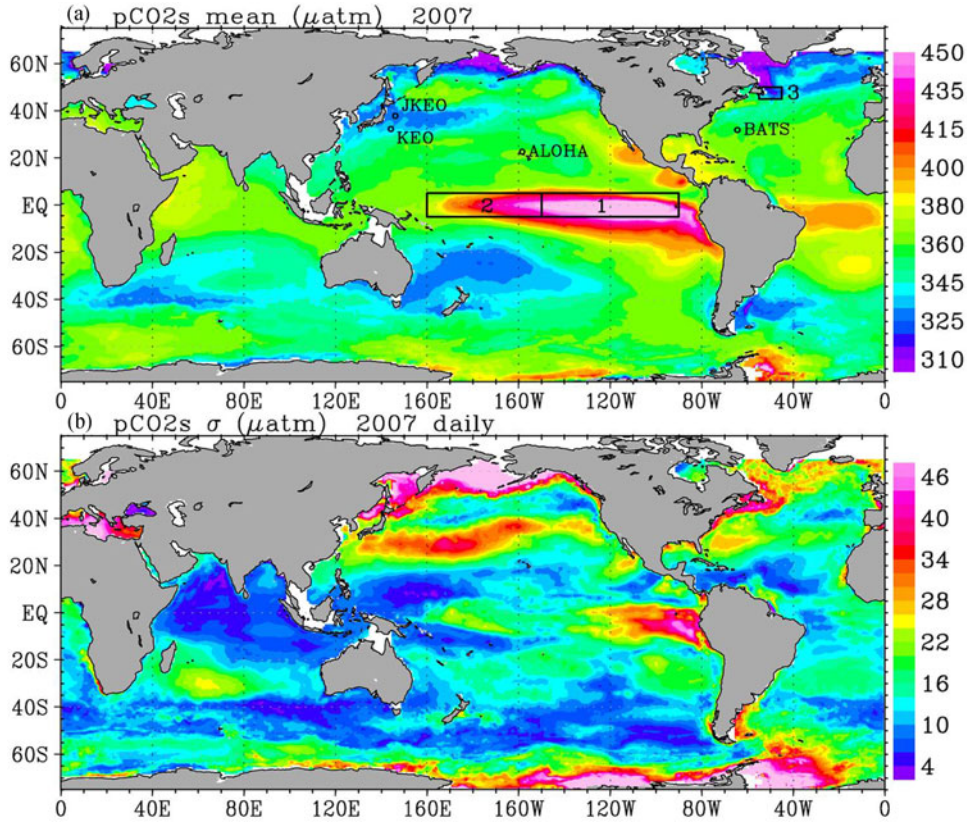

Fig. 2. Maps of 2007 pCO_2s for (a) yearly mean and (b) standard deviation of daily model outputs. The boxes in (a) are explained in Section VII. The stations marked in (a) are identified in Section IV.

Extension Observatory (JKEO) at 38 °N, 146.6 °E, with much shorter time series were also used to illustrate the latitudinal change of governing factors.

V. Related Space-Based Data

Microwave radiometers at certain frequencies have the advantage of measuring SST uninterrupted by cloud and water vapor contamination [44]. Despite early calibration problems of the Scanning Multichannel Microwave Radiometer, Liu [45], [46] was able to use the sensor to observe El Niño changes and to estimate ocean surface latent heat flux. Continuous measurements over the tropical oceans have been provided by the Tropical Rainfall Measuring Mission Microwave Imager (TMI) between 1997 and 2015. TMI used only the 11-GHz channel to retrieve SST; this channel is less sensitive in the cold water of high-latitude oceans [47]. The Advanced Microwave Scanning Radiometer for the Earth Observing System (AMSR-E), on board NASA's Aqua satellite, was launched in May 2002. It has global coverage and an additional channel at 7 GHz to optimize SST retrieval in cold water. SST from AMSR-E, averaged to 0.25° by 0.25° grids for ascending and descending paths, was obtained from Remote Sensing Systems [48] and used in this study.

For several decades, chlorophyll concentration based on remotely sensed variations in ocean color have been used to derive global phytoplankton productivity, e.g., [49]. Explicit representation of physiological processes remains elusive in primary production models [50], but variable chlorophyll florescence measured by space-based sensors is the most sensitive signal detectable in the upper ocean that reflects instantaneous photophysiology of phytoplankton. The signal to noise ratio of such measurements has been found to be low in oligotrophic regions [51]. Chl-*a* data we used were derived from a combination of measurements by the Sea-viewing Wide Field-of-view Sensor (SeaWiFS) and the Moderate-Resolution Imaging Spectroradiometer (MODIS) on both Terra and Aqua [52]. The daily Level 3 standard mapped image product has a spatial resolution of 9 km. Because clouds, aerosols, and sunlight availability affect the MODIS measurements, large data gaps exist on the daily maps. Both spatial and temporal smoothing/averaging were applied to the Chl-*a* data to fill data gaps.

VI. Statistical Model and Validation

A statistical model has been developed to retrieve pCO_2s from space-based observations using SVR. The training data are constructed as follows. The target data are daily averages computed from combined *in situ* pCO_2s observations over the global oceans as described in Section IV. Only data starting from 2002, with collocated satellite data have been used in developing the statistical model. The input data include satellite

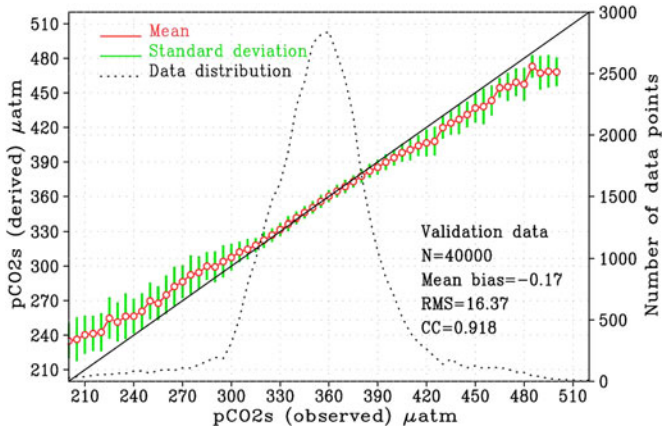

Fig. 3. Bin-averaged pCO_2s from model versus observed pCO_2s. 40000 randomly selected observations for 2002–2010, independent from data used to train the statistical model are used. Standard deviation is superimposed on each bin average as error bars.

data described in Section V, which are daily averages of collocated SST from AMSR-E and Chl-*a* from SeaWiFS/MODIS. Climatological SSS data [53] were also used in training. The day of year, longitude, and latitude were also included in the training as inputs. Time and longitude are taken in the forms of sine and cosine because of their periodicity. The input parameters and the target data (x), except for time and longitude, are normalized as: $x' = (x - \bar{x})/\sigma$ where $\bar{x}$ and σ are the mean and standard deviation of x.

After we reserved a set of 40 000 randomly selected data groups from the total dataset described in Sections IV and V for validation, we randomly selected another 40 000 data groups to train the model. With the model, nine years (2002–2011) of pCO_2s, at 0.5° and daily resolutions are produced. The maps for one year (2007) are shown in Fig. 2 as an example. They are in general agreement with climatology [17]. The yearly means have high values just south of the equator in the Pacific and Atlantic Oceans and low values over the western boundary currents. The standard deviations of the daily data show coherent patterns that require further analysis.

The validation is shown in Fig. 3. For the 40 000 data pairs at 0.5° and daily resolution, the mean difference between model predictions and measurements is –0.17 μatm and the RMS difference is 16.37 μatm; the latter is 6% of the data range of approximately 270 μatm. Assuming 28° of freedom, the RMS error of daily data is equivalent to 3.1 μatm for a monthly mean. In actual practice, the decorrelation time scale would be longer than a day, and the RMS error for monthly mean would likely be between 3.1 and 16.37 μatm. As a common problem to computation of turbulent flux through bulk parameterization, ΔpCO_2 required to compute the flux is a small difference between to two large values, and may require more stringent accuracy than available for pCO_2a or pCO_2s, depending on location and time [54]. Fig. 3 also shows the well-known "attenuation effect" of optimization—the model output overestimates in low range and underestimates in high range [55]. The number of data in these bins also is dramatically less in the low and high ranges, as shown in the figure. Because the RMS error is calculated using squared differences, it tends to be over weighted by the small numbers of outlying estimates with large biases at the low and high ranges. If we take the mean absolute error (MAE), an average of the absolute errors between the predicted and the true values, the error estimate equally weights each data point. The MAE for the validation is 9.68 μatm or 3.6% of the data range at daily timescale.

VII. Characterizing the Variability

A. Region of Influence

As described in Section II, there is a history of relating pCO_2s to SST and Chl-*a*. The nine years of pCO_2s from the model coincident with satellite data allow us to map the correlation coefficients shown in Fig. 4. Monthly means were used and only coefficients that meet 95% confidence level are shown. The coefficients have coherent zonal bands of positive and negative values in the Pacific and Atlantic Ocean. There are large uncertainties of our model over the Indian Ocean because the lack of data to train the model (see Fig 1). Over the equatorial oceans, pCO_2s correlates negatively with SST, but positively with Chl-*a*. Over most of high-latitude oceans pCO_2s correlated negatively with both Chl-*a* and SST. Over a wide spread of subtropical ocean, there are strong positive correlation between pCO_2s and SST. More comparison of changes between pCO_2s and the parameters will follow below.

Brix *et al*. [56] provided global maps of pCO_2s from numerical models by combining the Estimating the Circulation and Climate of the Ocean Phase II ($ECCO_2$), which provides the time-evolving physical ocean state, and the Darwin model, which provides time-evolving ocean ecosystem variables. Our outputs were demonstrated to be significantly better than their results when compared with *in situ* measurements over oligotrophic subtropical oceans [20].

B. Annual Cycle

In the subtropical oceans, the annual variations of the model outputs at Aloha and Bermuda stations agree well with HOT and BATS measurements, as shown in time series comparisons of Fig. 5. For BATS, the mean and standard deviation of the difference between the two time series are -6.9 and 15.3 μatm, respectively. The standard deviation is 16% of the annual range of 93.5 μatm for measurements. For HOT, the mean and standard deviation of the difference are 6.0 and 8.2 μatm. The standard deviation is 22% of the annual range of 37.3 μatm for measurements. The annual ranges of model outputs are 71.4 and 34.4 μatm at BATS and HOT, respectively. The annual ranges of the model outputs are smaller than the ranges of the observations. These differences in annual ranges are likely to be the manifestation of overestimation at low end and underestimation at high end shown in Fig. 3.

The measurements increase at rates of 2.0 and 1.7 μatm per year for BATS and HOT, respectively. Similar trends have been observed for different periods [57], [42], which may reflect the accumulation of CO_2 in the atmosphere. No significant trend is found in the model outputs within the nine years period. The

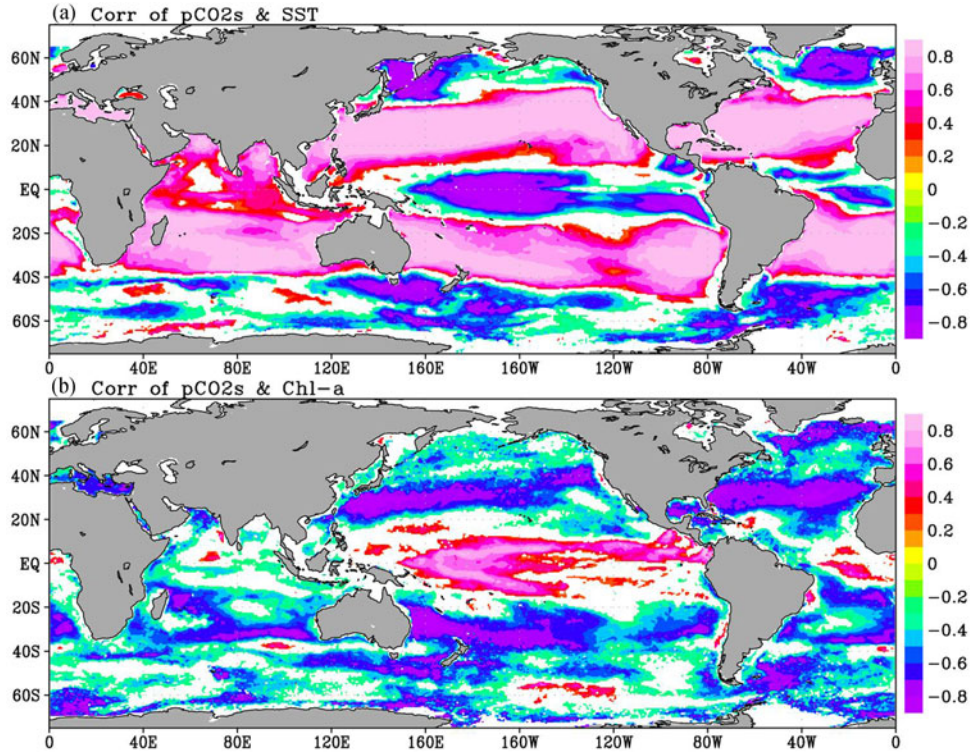

Fig. 4. Correlation coefficient between (a) pCO_2s and SST, and (b) pCO_2s and Chl-*a*, calculated from the 112 monthly data. Only those above the 95% confidence level are plotted.

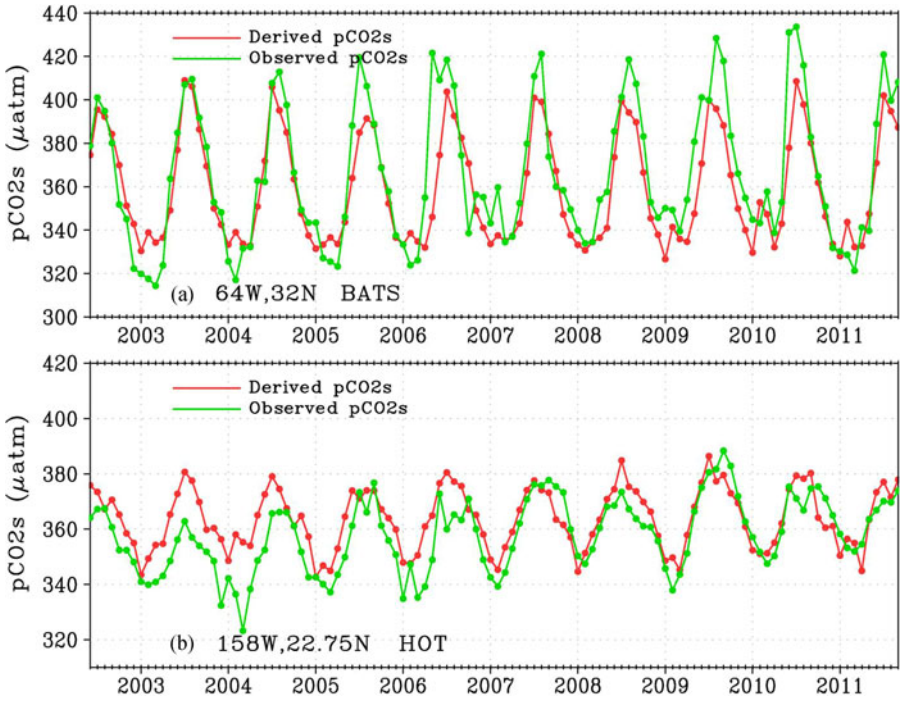

Fig. 5. Comparing nine years of monthly pCO_2s measured (green) at Station (a) BATS, and (b) ALOHA with model outputs (red).

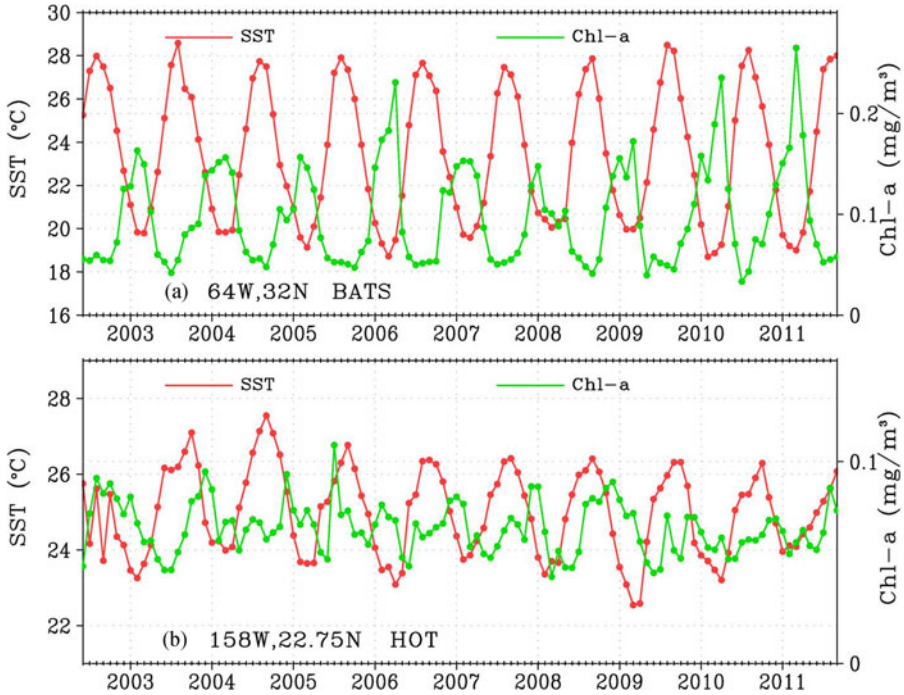

Fig. 6. Same as Fig. 5 but for SST (red) and Chl-*a* (green).

time series of the two inputs to compute pCO_2s, SST, and Chl-*a*, shown in Fig. 6, show no significant trend and that may explain the failure to produce significant trends in pCO_2s model outputs. The annual variations of pCO_2s are approximately in phase with SST, but not with Chl-*a*. SST is a more dominant factor than Chl-*a* in the annual variation of pCO_2s.

Another driver in addition to SST is needed going to extratropical oceans, as illustrated in the seasonal and latitudinal variations along 148 °E in North Pacific (in proximity of stations KEO and JKEO) of Fig. 7. The nine-year mean pCO_2s from model output [see Fig. 7(a)] agrees well with Takahashi climatology [36] [see Fig. 7(b)]. The climatology was linearly interpolated to model output resolution. South of 34 °N in the subtropical ocean, pCO_2s has an annual cycle, high in summer and low in winter, in phase with SST [see Fig. 7(c)]. North of this latitude in the extratropical oceans, there are two lows in pCO_2s, in April–May and in September–October, correspond to high Chl-*a* [see Fig. 7(d)]. Stronger biological productivity depletes CO_2. Biological processes are significant at higher latitudes while the physical–chemical processes dominate in subtropical oceans for changes in pCO_2s. West of this longitude, there is no climatology data available at extratropical latitudes, but there are two stations, KEO and JKEO south and north of 34 °N.

Figs. 8 and 9 show that the model outputs agree well with measurements at KEO and JKEO, although only short periods of measurements were accessible. At KEO to the south (see Fig. 8), the annual variations of pCO_2s agree well with SST, but they do not follow the semiannual variations of Chl-*a*. At JKEO to the north (see Fig. 9), pCO_2s has two cycles a year in opposite phase with Chl-*a*, but SST has only one cycle per year. The nine-year time series of pCO_2s from our model and the satellite data (SST and Chl-*a*) at these locations do not show significant trends, in consistent with the model outputs and satellite data at the Aloha and Bermuda stations.

C. Spring Bloom

As demonstrated in Figs. 7–9, ocean biological productivity becomes an important factor for pCO_2s at higher latitudes. The conventional hypothesis is that ocean vertical mixing brings nutrients to the surface during winter. Increasing sunlight during spring allows strong increase in photosynthesis that depletes surface CO_2. We examine several arbitrarily chosen 5°–10° latitude–longitude boxes in the North Atlantic Ocean to find cruise measurements (in the dataset described in Section IV) of pCO_2s. Fig. 10 shows an example in a region (45 °N–50 °N, 45 °W–55 °W) in 2007, where a reasonable number of cruise measurements covering the spring bloom are found. The region is marked by box 3 in Fig. 2(a). The time series at daily resolution shows a large drop in pCO_2s from the model in spring and a small drop in autumn, in agreement with the scattered cruise measurements, and corresponding to the rise of Chl-*a*. These spring and autumn signals are also observed in the high latitude Pacific, as shown in Fig. 7.

D. Interannual Anomalies of El Niño

As we approach the equator from the subtropics, vertical advection and upwelling in the ocean become increasingly important, bringing cold and CO_2-rich water to the surface. A negative correlation between pCO_2s and SST has been found

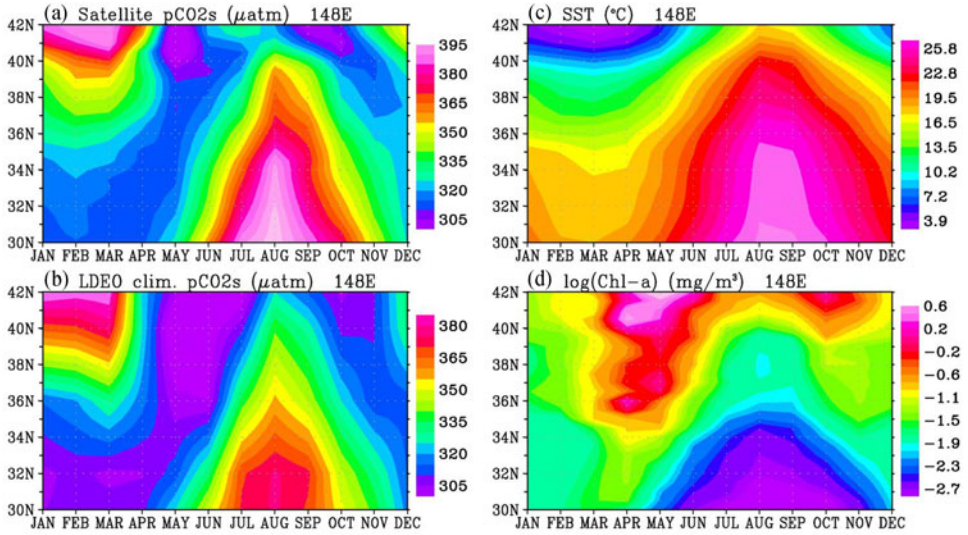

Fig. 7. Latitudinal-time variation along 148 °E in North Pacific: (a) pCO_2s from model output; (b) pCO_2s from Takahashi *et al*. climatology data averaged over the 2003–2010 period; (c) and (d) the same as (b), except for SST and log (Chl-*a*).

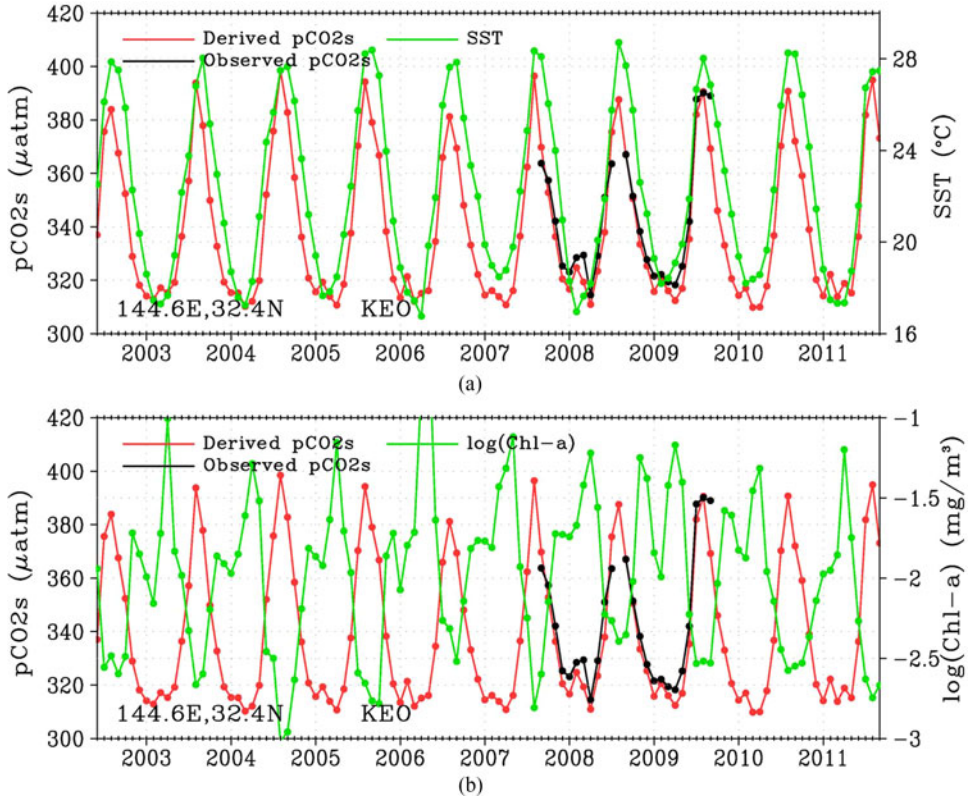

Fig. 8. Time series of pCO_2s from model (red) and observation (black) at KEO, compared with (a) SST (green) and (b) log (Chl-*a*) (green).

[25], [58]. The negative relation is more pronounced in the interannual episodes of El Niño warming and La Niña cooling in the equatorial Pacific [59], [60].

The conventional El Niño indices are represented by interannual SST anomalies (with the climatological annual cycle removed) at two regions centered on the equator in the Pacific. They are Niño 3, between 150 °W and 90 °W, and Niño 4, between 160 °E and 150 °W, as marked by boxes 1 and 2 in Fig. 2(a). The interannual anomalies of pCO_2s from our model, with annual cycle derived from the nine year of data removed, show opposite phases with the two El Niño indices in Fig. 11. Positive SST anomalies (El Niño) correspond to negative pCO_2s

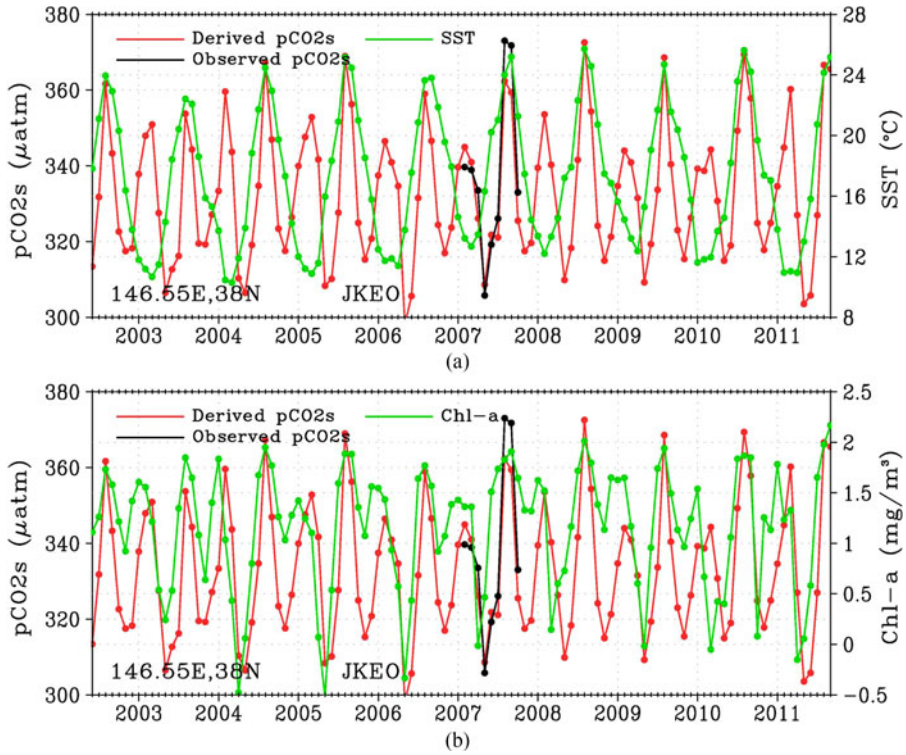

Fig. 9. Same as Fig. 8, except at JKEO.

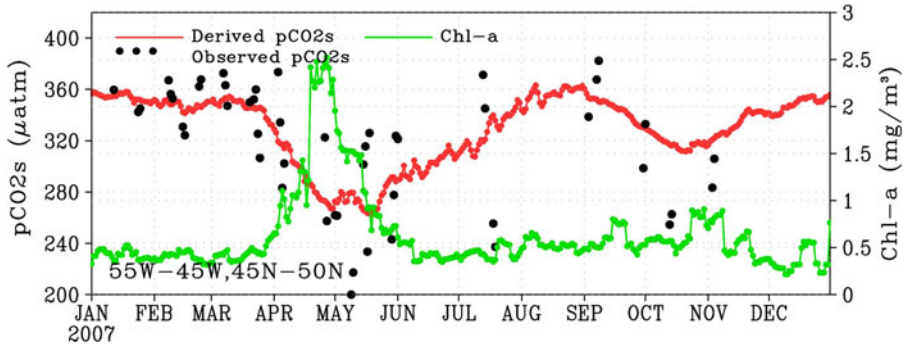

Fig. 10. Time series of pCO_2s from model output and Chl-*a* at daily resolution for 2007 for an area in North Atlantic. Measurements from ships are superimposed.

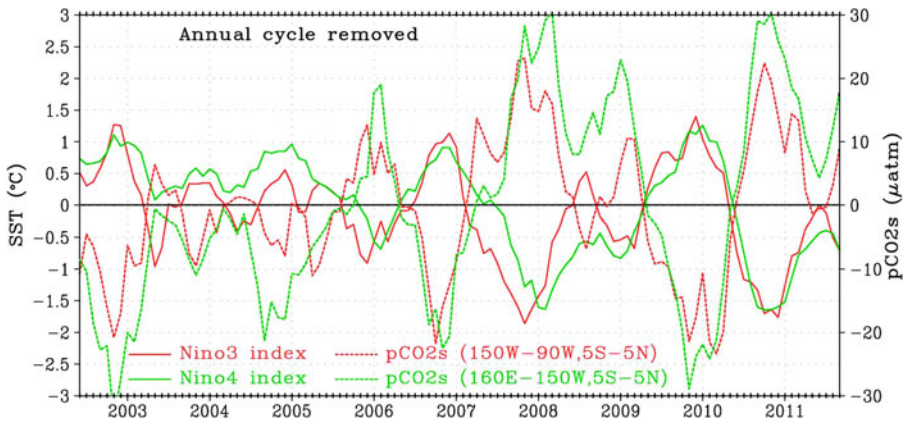

Fig. 11. Interannual anomalies of pCO_2s (dashed lines) from model outputs and El Niño indices (solid lines) at Niño 3 (red) and Niño 4 (green) regions.

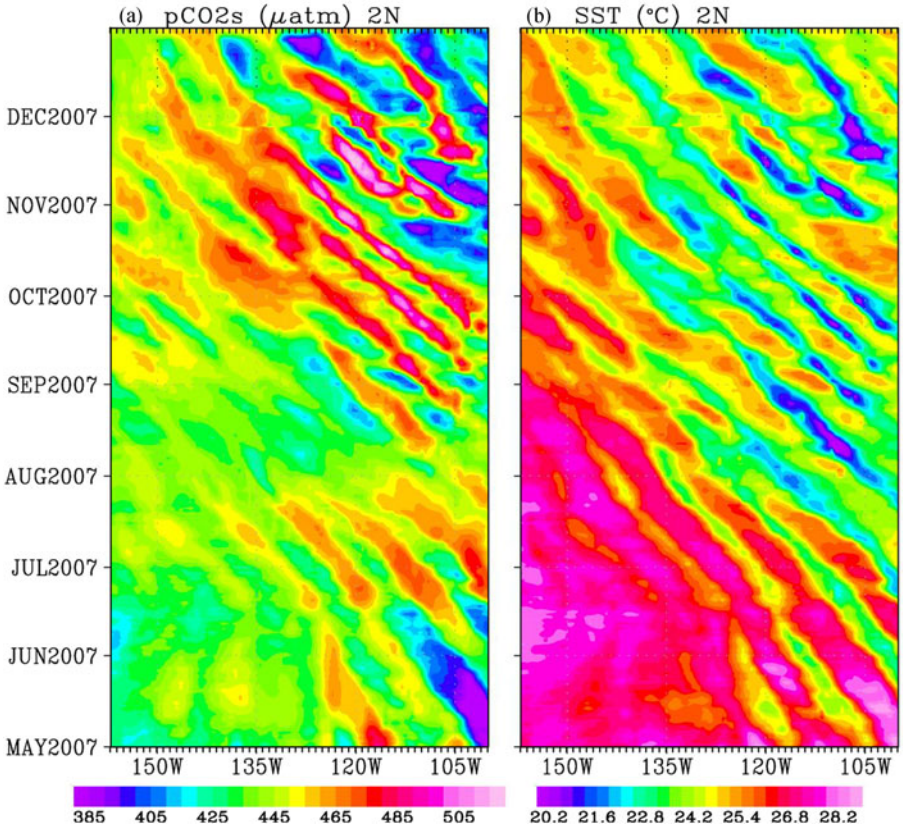

Fig. 12. Temporal and longitude variation at 2 °N in the Pacific for (a) pCO_2s from model output and (b) SST.

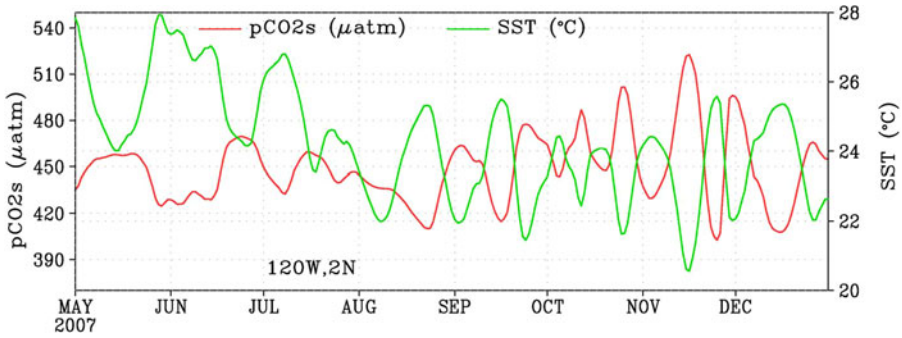

Fig. 13. Time series of pCO_2s (red) from model and SST (green) for 2007 at 2 °N and 120 °W showing the TIW.

anomalies (2002–2003, 2004–2005). This is in agreement with conventional knowledge, showing that our product picks up interannual anomalies.

E. High Frequency Variation due to TIW

In additional to the interannual episodes such as El Niño, a dominant feature in the equatorial oceans is the propagation of the intraseasonal TIW. TIWs vary in location and phase velocity. Such waves were best observed by radiometers on geostationary satellites as meanders of the temperature front between the cold upwelling water of the Pacific equatorial cold tongue and the warm water to the north [61], [62]. In general, the waves propagate westward, with period of approximately 30 days, wavelength of 1100 km, and phase speed of 0.5 m/s. The waves are stronger from June to November and during La Niña episodes. Their manifestation in wind vector [63]–[65], dynamic topography [66], biological processes [67], and surface salinity [68] has been observed.

The pCO_2s from the model clearly shows the manifestation of TIWs: the data in 2007 are shown as an example in Fig. 12. High SST corresponds to low pCO_2s. At 2 °N, both signals propagate westward approximately at same speed and period and these factors vary with latitude. Both signals are stronger in fall/winter than spring/summer. The features are further illustrated by the time series at 120 °W in Fig. 13. For 2007 at 2 °N from May to December, the speed and period of the TIWs are approximately 0.5 m/s and 30 days. The exception is found east of 130 °W

from August to October when the speed is approximately 0.65 m/s and the period is 20 days. The spatial scale is approximately 1000–1100 km along 2 °N.

VIII. Discussion

This study has demonstrated the feasibility of continuous coverage of pCO_2s over the global oceans for variability from a few days to a few years, using satellite data through a single statistical model. Our results confirm that SST is the dominant factor in pCO_2s changes, particularly in the subtropical oceans, and Chl-*a* becomes important at extratropical latitudes. Our data agree with measurements at ocean stations in magnitude and phase of the annual cycle. The dataset is shown to pick up the spring blooms at high latitudes, consistent with cruise measurements. The interannual anomalies of our data follow the known response to El Niño episodes. The westward propagations of our outputs closely follow the intraseasonal TIW.

The validation described in Section VI shows accuracy comparable to the regional regressions based on *in situ* measurements described in Section II. Such validation using ensemble data is only meaningful in regions with sufficient data. As is obvious in Fig. 1, large data gaps exist in the global oceans (e.g., Indian Ocean). Our model outputs track the seasonal variations in the tropical and extratropical oceans, but exhibit the well-known attenuation effect of optimization with overestimation in the low range and underestimation in high range. The result is a smaller seasonal range than *in situ* measurements.

The increase trend of atmospheric CO_2 is well observed, but our data fail to follow the increasing trend exhibited by the *in situ* measurements. The reason for the failure of our data to pick up pCO_2s trend is obvious. Our statistical model is driven only by satellite data. Neither the time series of SST nor Chl-*a*, which are the inputs to the model, show any significant trend. Long time series of satellite data are produced by merging data from different sensors with removal of systematic bias (and the possibility of removing real trend). Even without significant contribution to monitor the trend for greenhouse warming, the spatial-temporal variability provided by our data should be important to the characterization of ocean biogeochemistry and acidification.

In situ measurements of pCO_2s have been updated yearly. The latest report [69] indicated that an average of approximately 1.2 million ocean surface fCO_2 values per year for the years 2006 to 2012 were collected by SOCAT. The LEDO dataset was also updated [70]. Efforts to map *in situ* measurements were summarized [71]. New technology has allowed continuous autonomous measurements at moorings [72]. Our method to map pCO_2s does not require input and constant update of *in situ* data; we need only relative small amount of *in situ* measurements to train the model function and rely on satellite data to provide continuous global coverage. Only 40 000 randomly selected *in situ* data out of 250 000 we originally compiled were used. Nonetheless, new *in situ* data may improve distribution and will be very valuable in the training and validation of future statistical model.

This nine-year pCO_2s outputs we released for public access since 2014 [73] can be considered as a living dataset. The dataset has been continuously extended as new satellite sensors replace the old ones and the extended data are under evaluation. AMSR-2 on Global Change Observation Mission 1-Water (GCOM-W) has replaced AMSR-E. AMSR-2 data are well calibrated [74], [75]. Calibration and merging of SST products are also being conducted and coordinated by the Group for High Resolution Sea Surface Temperature (GHRSST) Project [76]. However, the continuous availability of the microwave radiometer with 7-GHz channel is uncertain after GCOM-W. Without measurement at this channel, the availability of SST and the derived pCO_2s with sufficient accuracy in the cold water of high-latitude oceans may be at risk. New data of Chl-*a* from the Second-generation Global Imager on GCOM-C [77] and the Visible Infrared Imaging Radiometer Suite onboard the Suomi National Polar-Orbiting Partnership (Suomi NPP) may also improve the outputs.

We built our model with salinity climatology before sufficient satellite measurements were available. Aquarius was launched in 2011 and measured SSS, covering the Earth's surface once every seven days, until its demise in 2015 [78]. The SSS data have 1° resolution. The Soil Moisture and Ocean Salinity, launched in November 2009, has provided global SSS measurements with three days revisits [79]. SSS is also retrieved from the Soil Moisture Active and Passive launched in 2015 [80]. These data will be incorporated in the revision of our statistical model and the effect of salinity on pCO_2s will be examined. SSS and SST are the important links between the water and carbon cycles.

Acknowledgment

This research was carried out at the Jet Propulsion Laboratory, California Institute of Technology, under a contract with the National Aeronautics and Space Administration. N. R. Bates kindly assisted the authors in using BATS data. The Japanese Space Exploration Agency provided valuable information and data during this study.

References

[1] D. J. Hoffmann, J. H. Butler, and P. Tans, "A new look at atmospheric carbon dioxide," *Atmos. Envirn.*, vol. 43, 2009, Art. no. 2084.

[2] C. Le Quere *et al.*, "Global carbon budget," *Earth Syst. Sci. Data*, vol. 7, pp. 349–396, 2015, doi: 10.519/rssd-7-3492015.

[3] A. Körtzinger, "Determination of carbon dioxide partial pressure (pCO_2)," in *Methods of Seawater Analysis*, 3rd ed., K. Grasshoff, K. Kremling, and M. Ehrhardt, Eds. Weinheim, Germany: Wiley-VCH Verlag GmbH, 1999, pp. 149–158, doi: 10.1002/9783527613984.ch9.

[4] P. S. Liss and L. Merlivat, "Air-sea gas exchange rates: Introduction and synthesis," in *The Role of Air-Sea Exchange in Geochemical Cycling*, P. Buat-Ménart, Eds., Dordrecht, The Netherlands: D. Reidel Pub. Co., pp. 113–127, 1986.

[5] A. J. Watson *et al.*, "Tracking the variable North Atlantic sink for atmospheric CO_2," *Science*, vol. 326, pp. 1391–1393, 2009.

[6] R. Wanninkhof, "Relationship between wind speed and gas exchange over the ocean," *J. Geophys. Res.*, vol. 97, pp. 7373–7382, 1992.

[7] J. Boutin, J. Etcheto, L. Merlivat, and Y. Rangama, "Influence of gas exchange coefficient parameterisation on seasonal and regional variability of CO_2 air-sea fluxes," *Geophys. Res. Lett.*, vol. 29, no. 8, 2002, Art. no. 1182, doi: 10.1029/2001GL013872.

[8] M. E. Carr, W. Tang, and W. T. Liu, "CO_2 exchange coefficients from remotely sensed wind speed measurements: SSM/I versus QuikSCAT in 2000," *Geophys. Res. Lett.*, vol. 29, no. 15, 2002, doi: 10.1029/2002GL015068.

[9] W. T. Liu, X. Xie, and W. Tang, "Scatterometer's unique capability in measuring ocean surface stress," *Oceanography From Space*, V. Barale, J. Gower, and L. Alberotanza, Eds. Berlin, Germany: Springer, 2010, pp. 93–111.

[10] D. M. Glover, N. M. Frew, S. J. McCue, and E. J. Bock, "A multi-year time series of global gas transfer velocity from the Topex dual frequency, normalized radar backscatter algorithm," in *Gas Transfer at Water Surfaces (Geophysical Monograph)*, vol. 127, M. A. Donelan, W. M. Drennan, E. S. Saltsman, and R. Wanninkhof, Eds. Washington, DC, USA: Amer. Geophys. Union, 2002, pp. 325–331.

[11] D. Bogucki, M.-E. Carr, W. M. Drennan, P. Woicesyn, T. Hara, and M. Schmeltz, "Preliminary and novel estimates of CO_2 gas transfer using a satellite scatterometer during the 2001 GasEx experiment," *Int. J. Remote Sens.*, vol. 31, pp. 75–92, 2010.

[12] N. Frew, "The role of organic films in air-sea gas exchange," in *The Sea Surface and Global Change*, P. S. Liss and R. A. Duce, Eds. New York, NY, USA: Cambridge Univ. Press, 1997, pp. 121–172.

[13] W.-T. Tsai and K.-K. Liu, "An assessment of the effect of sea surface surfactant on global atmosphere-ocean CO_2 flux," *J. Geophys. Res.*, vol. 108, no. C4, 2003, Art. no. 3127, doi: 10.1029/2000JC000740.

[14] I.-I. Lin, W. Alpers, and W. T. Liu, "First evidence for the detection of natural surface films by the scatterometer," *Geophys. Res. Lett.*, vol. 30, no. 13, Jul. 2003, Art. no. 1713, doi: 10.1029/2003GL017415.

[15] H. Hashizume and W. T. Liu, "Systematic error of microwave scatterometer wind related to the basin scale plankton bloom," *Geophys. Res. Lett.*, vol. 31, 2004, Art. no. L06307, doi: 10.1029/2003GTL01841.

[16] D. K. Woolf, "Bubbles and their role in gas exchange," in *The Sea Surface and Global Change*, P. S. Liss and R. A. Duce, Eds. Cambridge, U.K.: Cambridge Univ. Press, 1997, pp. 173–205.

[17] T. Takahashi *et al.*, "Global sea-air CO_2 flux based on climatological surface ocean pCO_2, and seasonal biological and temperature effects," *Deep-Sea Res. II*, vol. 49, pp. 1601–1622, 2002.

[18] A. Körtzinger, "Determination of carbon dioxide partial pressure (pCO_2)," in *Methods of Seawater Analysis*. Weinheim, Germany: VerlagChemie, 1999, pp. 149–158.

[19] A. G. Dickson and C. Goyet, Handbook of Methods for the Analysis of the Various Parameters of the Carbon Dioxide System in Sea Water, vol. 2, Versions 2, U.S. Dept. Energy, Oak Ridge, TN, USA, 1997.

[20] W. T. Liu and X. Xie, "Ocean surface carbon dioxide fugacity observed from space," Jet Propulsion Lab., California Inst. Tech., Pasadena, CA, USA, JPL-Publ.-14-15, 2014.

[21] M. P. Stephens, G. Samuels, D. B. Olson, R. A. Fine, and T. Takahashi, "Sea-air flux of CO_2 in the North Pacific using shipboard and satellite data," *J. Geophys. Res.*, vol. 100, pp. 13571–13583, 1995.

[22] C. Goyet, F. J. Millero, D. W. O'Sullivan, G. Eischeid, S. J. McCue, and R. G. J. Bellerby, "Temporal variations of pCO_2 in surface seawater of the Arabian Sea in 1995," *Deep-Sea Res. I*, vol. 45, pp. 609–623, 1998.

[23] E. M. Hood, L. Merlivat, and T. Johannessen, "Variations of fCO_2 and air–sea flux of CO_2 in the Greenland Sea gyre using high-frequency time series data from CARIOCA drift buoys," *J. Geophys. Res.*, vol. 104, pp. 20571–20583, 1999.

[24] N. B. Nelson, N. R. Bates, D. A. Siegel, and A. F. Michaels, "Spatial variability of the CO_2 sink in the Sargasso Sea," *Deep-Sea Res. II*, vol. 48, pp. 1801–1821, 2001.

[25] C. E. Cosca *et al.*, "Seasonal and interannual CO_2 fluxes for the central and eastern equatorial Pacific Ocean as determined from fCO_2-SST relationships," *J. Geophys. Res.*, vol. 108, no. C8, 2003, Art. no. 3278, doi: 10.1029/2000JC000677.

[26] T. Ono, T. Saino, N. Kurita, and K. Sasaki, "Basin-scale extrapolation of shipboard pCO_2 data by using satellite SST and Chl*a*," *Int. J. Remote Sens.*, vol. 25, no. 19, pp. 3803–3815, 2004.

[27] Y. Zhu, S. Shang, W. Zhai, and M. Dai, "Satellite-derived surface water pCO_2 and air–sea CO_2 fluxes in the northern South China Sea in summer," *Progress Nat. Sci.*, vol. 19, pp. 775–779, 2009.

[28] V. V. S. S. Sarma *et al.*, "Basin-scale pCO_2 distribution using satellite sea surface temperature, Chl *a*, and climatological salinity in the North Pacific in spring and summer," *Global Biogeochem. Cycles*, vol. 20, 2006, Art. no. GB3005, doi: 10.1029/2005GB002594.

[29] X. A. Padin, G. Navarro, M. Gilcoto, A. F. Rios, and F. F. Perez, "Estimation of air-sea CO_2 fluxes in the Bay of Biscay based on empirical relationships and remotely sensed observations," *J. Mar. Syst.*, vol. 75, pp. 280–289, 2009.

[30] N. Lefevre, A. J. Watson, and A. R. Watson, "A comparison of multiple regression and neural network techniques for mapping in situ pCO_2 data," *Tellus B*, vol. 57, pp. 375–384, doi: 10.1111/j.1600-0889.2005.00164.x, 2005.

[31] M. Telszewski *et al.*, "Estimating the monthly pCO_2 distribution in the North Atlantic using a self-organizing neural network," *Biogeosciences*, vol. 6, pp. 1405–1421, 2009, doi: 10.5194/bg-6-1405–2009.

[32] T. Friedrich and A. Oschlies, "Neural network-based estimates of North Atlantic surface pCO_2 from satellite data: A methodological study," *J. Geophys. Res.*, vol. 114, 2009, Art. no. C03020, doi: 10.1029/2007JC004646.

[33] A. J. Smola and B. Schölkopf, "A tutorial on support vector regression," *Statist. Comput.*, vol. 14, pp. 199–222, 2004.

[34] X. Xie, W. T. Liu, and B. Tang, "Spacebased estimation of moisture transport in marine atmosphere using support vector machine," *Remote Sens. Environ.*, vol. 112, pp. 1846–1855, 2008.

[35] V. N. Vapnik, *Nature of Statistical Learning Theory*. Berlin, Germany: Springer, 1995.

[36] T. Takahashi, S. C. Sutherland, and A. Kozyr, "Global ocean surface water partial pressure of CO_2 Database: Measurements performed during 1957–2012 (Version 2012)," U.S. Dept. Energy, Carbon Dioxide Inf. Analysis Center, Oak Ridge Nat. Lab., Oak Ridge, TN, USA, ORNL/CDIAC-160, NDP-088(V2012), 2013, doi: 10.3334/CDIAC/OTG.NDP088(V2012).

[37] R. M. Key *et al.*, "The CARINA data synthesis project: Introduction and overview," *Earth Syst. Sci. Data*, vol. 2, no. 1, pp. 105–121, 2010.

[38] D. Pierrot *et al.*, "CARINA TCO_2 data in the Atlantic Ocean," *Earth Syst. Sci. Data*, vol. 3, pp. 1–26, 2010.

[39] E. Lewis and D. W. R. Wallace, "Program developed for CO_2 system calculations," U.S. Dept. Energy, Carbon Dioxide Inf. Anal. Center, Oak Ridge Nat. Lab., Oak Ridge, TN, USA, ORNL/CDIAC-105, 1998.

[40] X. Xie and W. T. Liu, "Spacebased carbon dioxide fugacity in sea," *presented at the Joint IMBER/SOLAS Synthesis Meeting UNESCO Paris*, Sep. 12–16, 2011. [Online]. Available: https://airsea.jpl.nasa.gov/publication/paper/Xie-Liu-2011-unesco.pdf

[41] B. Pfeil *et al.*, "A uniform, quality controlled surface ocean CO_2 atlas (SOCAT)," *Earth Syst. Sci. Data*, vol. 5, pp. 125–143, 2013, doi: 10.5194/essd-5-125-2013.

[42] J. E. Dore, R. Lukas, D. W. Sadler, M. J. Church, and D. M. Karl, "Physical and biogeochemical modulation of ocean acidification in the central North Pacific," *Proc. Nat. Acad. Sci. USA*, vol. 106, pp. 12235–12240, 2009.

[43] N. R. Bates, M. W. Lomas, and R. J. Johnson, "The Bermuda Atlantic Time-series Study (BATS) enters its twenty-fifth year of ocean observations in the North Atlantic that illustrate change in ocean carbon," *Ocean Carbon Biogeochem. News*, vol. 6, no. 2, pp. 7–11, 2013.

[44] F. J. Wentz, C. L. Gentemann, D. R. Smith, and D. B. Chelton, "Satellite measurement of sea surface temperature through clouds," *Science*, vol. 288, no. 5467, pp. 847–850, 2000.

[45] W. T. Liu, "1982-1983 El Nino Atlas - Nimbus-7 microwave radiometer data," Jet Propulsion Lab., California Inst. Tech., Pasadena, CA, USA, JPL-Publ-87-5, 1987, pp. 68.

[46] W. T. Liu, "Remote Sensing of surface turbulence flux," in *Surface Waves and Fluxes*, vol. II, G. L. Geenaert and W. J. Plant Eds. Norwell, MA, USA, Kluwer, 1990, ch. 16, pp. 293–309.

[47] C. L. Gentemann, T. Meissner, and F. J. Wentz, "Accuracy of satellite sea surface temperature at 7 and 11 GHz," *IEEE Trans. Geosci. Remote Sens.*, vol. 48, no. 3, pp. 1009–1018, Mar. 2010.

[48] F. J. Wentz and T. Meissner, "AMSR Ocean Algorithm, Version 2," Remote Sens. Syst., Santa Rosa, CA, USA, RSS Tech. Rep. 121599A, 1999.

[49] D. Antoine, J.-M. Andre, and A. Morel, "Oceanic primary production 2. Estimation at global scale from satellite (coastal zone color scanner) chlorophyll," *Global Biogeochemical Cycles*, vol. 10, pp. 57–69, 1996.

[50] M. J. Behrenfeld, E. Boss, D. A. Siegel, and D. M. Shea, "Carbon-based ocean productivity and phytoplankton physiology from space," *Global Biogeochem. Cycles*, vol. 19, 2005, Art. no. GB1006, doi: 10.1029/2004GB002299.

[51] H. Lin, F. I. Kuzminov, J. Park, S. Lee, P. G. Falkowski, and M. Y. Gorbunov, "The fate of photons absorbed by phytoplankton in the global ocean," *Science*, vol. 351, no. 6270, pp. 264–267.

[52] J. E. O'Reilly *et al.*, "Ocean color chlorophyll algorithms for SeaWiFS," *J. Geophys. Res.*, vol. 103, pp. 24937–24953, 1998, doi: 10.1029/98JC02160.

[53] T. Boyer, S. Levitus, H. Garcia, R. A. Locarnini, C. Stephens, and J. Antonov, "Objective analyses of annual, seasonal, and monthly temperature and salinity for the world ocean on a 0.25 degree grid," *Int. J. Clim.*, vol. 25, pp. 931–945, 2005.

[54] T. Takahasshi *et al.*, "Climatological mean and decadal change in surface ocean pCO_2, and net sea-air CO_2 flux over the global oceans," *Deep Sea Res. II*, vol. 56, pp. 554–557, 2009.

[55] W. A. Fuller, *Measurement Error Models*, Hoboken, NJ, USA: Wiley, 1987, p. 440.

[56] H. Brix *et al.*, "Using Green's Functions to initialize and adjust a global, eddying ocean biogeochemistry general circulation," *Ocean Model.*, vol. 95, pp. 1–14, 2015.
[57] N. R. Bates, "Interannual variability of the oceanic CO_2 sinkin the subtropical gyre of the North Atlantic Ocean over the last two decades," *J. Geophys. Res.-Oceans*, vol. 112, 2007, Art. no. C09013, doi: 10.1029/2006JC003759.
[58] J. Boutin *et al.*, "Satellite sea surface temperature: a powerful tool for interpreting in situ pCO_2 measurements in the equatorial Pacific Ocean," *Tellus*, vol. 51B, pp. 490–508, 1999.
[59] R. Wannikhof *et al.*, "Surface water fCO_2 in the eastern equatorial Pacific during the 1992-1993 El Nino," *J. Geophys. Res.*, vol. 101, no. C7, pp. 16333–26343, 1996.
[60] R. A. Feely *et al.*, "Seasonal and interannual variability of CO_2 in the equatorial Pacific," *Deep-Sea Res. II*, vol. 49, pp. 2443–2460, 2002.
[61] R. Legeckis, "Long waves in the eastern equatorial Pacific Ocean: A view from a geostationary satellite," *Science*, vol. 197, pp. 1179–1181, 1997.
[62] J. A. Yoder, S. G. Ackleson, R. T. Barber, P. Flament, and W. M. Balch, "A line in the sea," *Nature*, vol. 371, pp. 689–692, 1994.
[63] S. P. Xie, M. Ishiwatari, H. Hashizume, and K. Takeuchi, "Coupled ocean-atmospheric waves on the equatorial front," *Geophys. Res. Lett.*, vol. 25, pp. 3863–3966, 1998.
[64] W. T. Liu, X. Xie, P. S. Polito, S. Xie, and H. Hashizume, "Atmosphere manifestation of tropical instability waves observed by QuikSCAT and Tropical Rain measuring missions," *Geophys. Res. Lett.*, vol. 27, pp. 2545–2548, 2000.
[65] D. B. Chelton and Coauthors, "Observations of coupling between surface wind stress and sea surface temperature in the eastern tropical Pacific," *J. Clim.*, vol. 14, pp. 1479–1498, 2001.
[66] P. Polito, J. P. Ryan, W. T. Liu, and F. P. Chavez, "Oceanic and atmospheric anomalies of tropical instability waves," *Geophys. Res. Lett.*, vol. 28, pp. 2233–2236, 2001.
[67] F. P. Chavez *et al.*, "Biological and chemical response of the equatorial pacific to the 1997-98 E1 Nino," *Science*, vol. 286, pp. 2126–2131, 1999.
[68] T. Lee, G. Lagerloef, M. M. Gierach, H.-Y. Kao, S. Yueh, and K. Dohan, "Aquarius reveals salinity structure of tropical instability waves," *Geophys. Res. Lett.*, vol. 39, 2012, Art. no. L12610, doi: 10.1029/2012GL052232.
[69] D. Bakker *et al.*, "An update to the surface ocean CO_2 atlas (SOCAT version 2)," *Earth Syst. Sci. Data*, vol. 6, pp. 69–90, 2013.
[70] T. Takahashi, S. C. Sutherland, and A. Kozyr, "Global ocean surface water partial pressure of CO_2 database: Measurements performed during 1957-2015 (Version 2015)," U.S. Dept. Energy, Carbon Dioxide Inf. Anal. Center, Oak Ridge Nat. Lab., ORNL/CDIAC-160, NDP-088(V2015), Oak Ridge, TN, USA, 2016, doi: 10.3334/CDIAC/OTG.NDP088(V2015).
[71] C. Rodenbeck *et al.*, "Data-based estimates of the ocean carbon sink variability—First results of the Surface Ocean pCO_2 Mapping intercomparison (SOCOM)," *Biogeosciences*, vol. 12, pp. 7251–7278, 2015, doi: 10.5194/bg-12-7251-2015.
[72] A. J. Sutton *et al.*, "A high frequency atmospheric and sea water pCO_2 data set from 14 open ocean sites using a moored autonomous system," *Earth Sys. Sci. Data*, vol. 6, pp. 353–366, 2014, doi: 10.5194/essd-6-353-2014.
[73] [Online]. Available: https://airsea.jpl.nasa.gov/seaflux/carbon-flux.html
[74] C. L. Gentemann and K. Hilburn, "In situ validation of sea surface temperatures from the GCOM-W1 AMSR2 RSS calibrated brightness temperatures," *J. Geophys. Res. Oceans*, vol. 120, no. 5, pp. 3567–3585, 2015, doi: 10.1002/2014JC010574.
[75] T. Hihara, M. Kubota, and A. Okuro, "Evaluation of sea surface temperature and wind speed observed by GCOM-W1/AMSR2 using in situ data and global products," *Remote Sens. Environ.*, vol. 164, pp. 170–178, 2015, doi: 10.1016/j.rse.2015.04.005.
[76] C. J. Donlon *et al.*, "The GODAE high resolution sea surface temperature pilot project (GHRSST-PP)," *Oceanography*, vol. 22, no. 3, pp. 34–45, 2009.
[77] K. Imaoka *et al.*, "Global change observation mission (GCOM) for monitoring carbon, water cycles, and climate change," *Proc. IEEE*, vol. 98, no. 5, pp. 717–734, May 2010.
[78] G. Lagerloef, F. Wentz, S. Yeuh, H. Kao, G. Johnson, and J. Lyman, "Aquarius satellite mission provides new detailed view of sea surface salinity, in state of the climate in 2011," *Bull. Amer. Meteorol. Soc.*, vol. 93, no. 7, pp. S70–S71, 2012, doi: 10.1175/2012BAMSStateoftheClimate.1.
[79] S. Mecklenburg *et al.*, "ESA's soil moisture and ocean salinity mission–achievements and applications after more than 6 years in orbit," *Remote Sen. Environ.*, vol. 180, pp. 1–2, 2016. [Online]. Available: http://doi.org/10.1016/j.rse.2016.03.020
[80] A. G. Fore, S. H. Yueh, W. Tang, B. W. Stiles, and A. K. Hayashi, "Combined active/passive retrievals of ocean vector wind and sea surface salinity with SMAP," *IEEE Trans. Geosci. Remote Sens.*, vol. 54, no. 12, pp. 7396–7404, Dec. 2016, doi: 10.1109/TGRS.2016.2601486.

W. Timothy Liu received the B.S. degree (*summa cum laude*) in physics from Ohio University, Athens, OH, USA, in 1971, and the M.S. and Ph.D. degrees in atmospheric sciences from the University of Washington, Seattle, WA, USA, in 1974 and 1978, respectively.

In 1979, he was a Principle Investigator on studies concerning ocean–atmosphere interaction and satellite oceanography in the Jet Propulsion Laboratory (JPL), California Institute of Technology, Pasadena, CA, USA. In 1993, he became a Senior Research Scientist at JPL, which is equivalent to a Full Professor in major U.S. universities. He was the Project Scientist of three NASA scatterometer missions during 1992–2006.

Dr. Liu was with the editorial boards of several scientific journals and has been on the science teams of many U.S. and international space missions. He is a Fellow of the American Meteorological Society, the American Association for the Advancement of Science, and the American Geophysical Union. He received the AMS Verner E. Suomi Award in 2010.

Xiaosu Xie received the B.S. degree in fluid mechanics from Tsinghua University, Beijing, China, in 1987, the M.S. degree in atmospheric science from the Chinese Academy of Meteorological Science, Beijing, China, in 1990, and the Ph.D. degree in atmospheric science from the University of Hawaii, Honolulu, HI, USA, in 1995.

She was a Research Associate from 1996 to 1997 and has been a Research Scientist since 1997 at the Jet Propulsion Laboratory, California Institute of Technology, Pasadena, CA, USA.